JOURNAL OF GEOPHYSICAL RESEARCH, VOL. 114, E01001, doi:10.1029/2008JE003253, 2009

Surface morphology of domes in the Marius Hills and Mons Rümker regions of the Moon from Earth-based radar data

Bruce A. Campbell,[1] B. R. Hawke,[2] and Donald B. Campbell[3]

Received 18 August 2008; revised 7 October 2008; accepted 20 October 2008; published 15 January 2009.

[1] Clusters and coalesced complexes of domes represent a relatively rare landform within the extensive, low-relief, lunar maria. While they are typically spectroscopically similar to mare basalts emplaced by high-volume, low-viscosity eruptions, the large-scale morphology of the domes is more consistent with slower emplacement and/or more viscous magma. We use new Earth-based radar data to study the decimeter- to meter-scale rock abundance, at the surface and buried within the probing range of the radar signal, of domes in the Marius Hills and Mons Rümker regions. Domes of the Marius Hills are characterized by high circular polarization ratio (CPR) values at 12.6-cm and 70-cm wavelength, similar to the near-rim ejecta deposits of young lunar craters like Tycho, areas of large ejecta fragments near the rim of Meteor Crater, and blocky lavas such as SP flow in Arizona. We infer that a very rugged flow surface morphology, associated with the original dome-forming eruption rather than postemplacement modification, exists beneath at most a few meters of regolith. Magmas with greater silica content than sampled lunar basalts are unlikely, so the blocky structure of the dome-forming lava must arise from some combination of compositional change, effusion rate, and/or cooling effects not typically observed in basaltic landforms on the Earth. Much of the 80-km diameter Mons Rümker has low backscatter and CPR at 12.6-cm wavelength relative to nearby mare terrain. At 70-cm wavelength, the northern and most of the southern parts of the complex are radar dark, but there is a radar bright feature that extends from the central region eastward into Oceanus Procellarum. We conclude that much of Mons Rümker is mantled by rock-poor, fine-grained pyroclastic material; the radar bright feature in the 70-cm map is detectable owing to some combination of greater roughness (like the Marius domes) and thinner mantling cover.

Citation: Campbell, B. A., B. R. Hawke, and D. B. Campbell (2009), Surface morphology of domes in the Marius Hills and Mons Rümker regions of the Moon from Earth-based radar data, *J. Geophys. Res.*, *114*, E01001, doi:10.1029/2008JE003253.

1. Introduction

[2] Basalt flow complexes, or maria, fill most basins on the nearside of the Moon. These flood-like deposits were initially smooth at the meter and larger scale, and lobate fronts show that individual eruptions emplaced units up to a few tens of meters in thickness. Subsequent meteorite bombardment created more rugged, cratered topography, and developed a regolith of mixed dust and rock that increases in thickness with time. Evidence for eruptions of magma more viscous than the mare-forming flows, due either to slower eruption rates and associated cooling, increased initial silica content, or other mechanisms, is limited to a few clusters and coalesced complexes of domes.

[3] The largest collection of such domes occurs in the Marius Hills region of Oceanus Procellarum [*Whitford-Stark and Head*, 1977; *McCauley*, 1967] (Figure 1). These volcanic constructs occupy a few hundred meter high mare plateau, and appear to have formed in alternating episodes with the smoother surrounding flows [*Guest*, 1971; *Greeley*, 1971; *Heather et al.*, 2003]. Spectroscopic analysis based on Clementine ultraviolet visible light camera data suggests that the surfaces of the Marius domes are of similar composition to the mare units, while cones in the area have signatures consistent with mixtures of varying amounts of glass-rich and microlitic materials that suggest a pyroclastic origin [*Weitz and Head*, 1999; *Heather et al.*, 2003]. The large-scale morphology of the often steep-sided Marius domes is consistent with emplacement by more viscous lava. Most workers suggest, on the basis of studies of melt evolution, that such increased viscosity arises owing to eruptions of cooler, crystal-rich basaltic magma rather than more evolved, silica-rich material [e.g., *Rutherford et al.*, 1974].

[4] Mons Rümker is an 80-km diameter collection of coalesced domes and associated thick flow features that

[1]Center for Earth and Planetary Studies, Smithsonian Institution, Washington, D.C., USA.
[2]School of Ocean and Earth Science and Technology, Hawai'i Institute of Geophysics and Planetology, University of Hawai'i, Honolulu, Hawaii, USA.
[3]Department of Astronomy, Cornell University, Ithaca, New York, USA.

0148-0227/09/2008JE003253$09.00

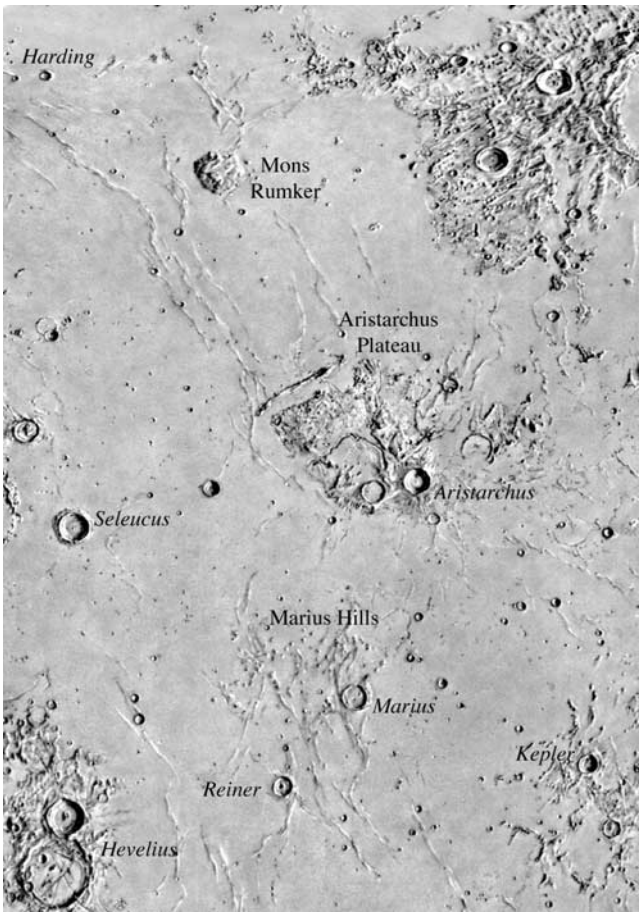

Figure 1. Shaded-relief view of the region from 0°–50°N, 290°–325°E, with major volcanic landforms noted. Craters are labeled in italics. A portion of the Iridum crater rim occurs at top right.

form an annular scarp at the boundary with the maria [*Guest*, 1971; *Scott and Eggleton*, 1973; *Smith*, 1974] (Figure 1). The northwest portion of this complex, and some outliers, appear to have formed atop premare, lineated deposits mapped as part of the Fra Mauro formation, but whether this unit occurs beneath the entire dome structure is uncertain [*Scott and Eggleton*, 1973]. While the Fra Mauro Formation is generally interpreted as ejecta deposits of Imbrium basin, it should be noted that the lineations in the northwestern portion of Mon Rümker trend east-northeast, and are thus not radial to Imbrium. These lineations are nearly radial to Iridum crater, and may be associated with the deposits of Iridum secondary craters mapped in the area by *Scott and Eggleton* [1973] and *Whitford-Stark and Head* [1977]. *Smith* [1974] noted that the lineated materials appear subdued relative to other mapped outcrops owing to "a thin deposit associated with volcanic activity in the southern part of the Rümker Hills."

[5] Radar backscatter measurements can provide significant new information on the surface and near-surface physical properties of the Marius and Rümker domes. In particular, the circular polarization ratio (CPR) is an indicator of the degree of diffuse scattering by wavelength-scale linear features (e.g., rock edges) or multiple scattering among rock faces that are relatively smooth at the wavelength scale (see Appendix). The radar data also provide a means to probe below the surface, with the penetration depth depending upon the illuminating wavelength and the composition of the regolith-forming material [e.g., *Carrier et al.*, 1991; *Campbell et al.*, 1997; *Campbell and Hawke*, 2005]. Such decimeter- to meter-scale morphologic information, in turn, is linked with the rheology and eruption rate of the dome-forming lavas. For example, terrestrial basalt flows exhibit a range of surface morphology (and CPR) with either greater viscosity or local flow rate, from gently rolling pahoehoe structure to rugged, platy a′a texture. More silicic magmas can form blocky deposits, made up of decimeter- to meter-scale smooth-sided boulders, which have diagnostic radar scattering properties [e.g., *Campbell et al.*, 1993; *Plaut et al.*, 2004].

[6] In this paper, we first describe new 12.6-cm and 70-cm wavelength Earth-based radar images and polarimetry data for the Marius Hills and Mons Rümker (section 2). These data are used to compare the surface and near-surface roughness of the Marius domes with mare flows and young crater deposits, and with terrestrial lava flows and crater ejecta imaged by the NASA/Jet Propulsion Laboratory (JPL) airborne synthetic aperture radar (AIRSAR) system (section 3). Section 4 presents similar Earth-based radar data for Mons Rümker, which has very different near-surface properties from the Marius Hills. On the basis of these results, we infer the original morphology of the dome-forming lava flows and discuss implications for local volcanic history, eruption mechanisms, and magma properties (section 5).

2. Radar Data Collection and Calibration

[7] We transmit a circular polarized signal from the Arecibo Observatory in Puerto Rico and receive both senses of the reflected echo from the Moon at the Green Bank Telescope in West Virginia. The 70-cm (430 MHz) data use a 3-μs pulsed signal and 17-min integration period to yield a spatial resolution of about 500 m per pixel. The 12.6-cm (2380 MHz) observations use a coded signal with a time resolution of 0.1 μs (range resolution of 15 m). The length of the integration period used for the two sites discussed here was 13 min, yielding a spatial resolution in the frequency axis of about 80 m per pixel, with 3 averaged "looks" in range. The raw data are processed using a focusing (synthetic aperture) algorithm to avoid smearing of areas distant from the location on the lunar surface used as a reference for time shifting and frequency shifting of the transmitted signal [*Campbell et al.*, 2007].

[8] At both wavelengths, we measure the receiver thermal noise power during times when no echo from the Moon is present. This allows for accurate calibration of the circular polarization ratio (μ_c or CPR), which is the ratio between the echo power in the same circular polarization sense (SC) as that transmitted to the echo power in the opposite circular sense (OC), $\mu_c = \sigma^0_{SC}/\sigma^0_{OC}$. CPR values are typically used to measure the degree of single-bounce diffuse scattering from rough surfaces or multiple-bounce echoes from rugged but locally facet-like terrain (Appendix A) [e.g., *Hagfors*, 1967]. The dimensionless backscatter coefficient (radar cross section per unit area), σ^0, is calibrated for the 70-cm

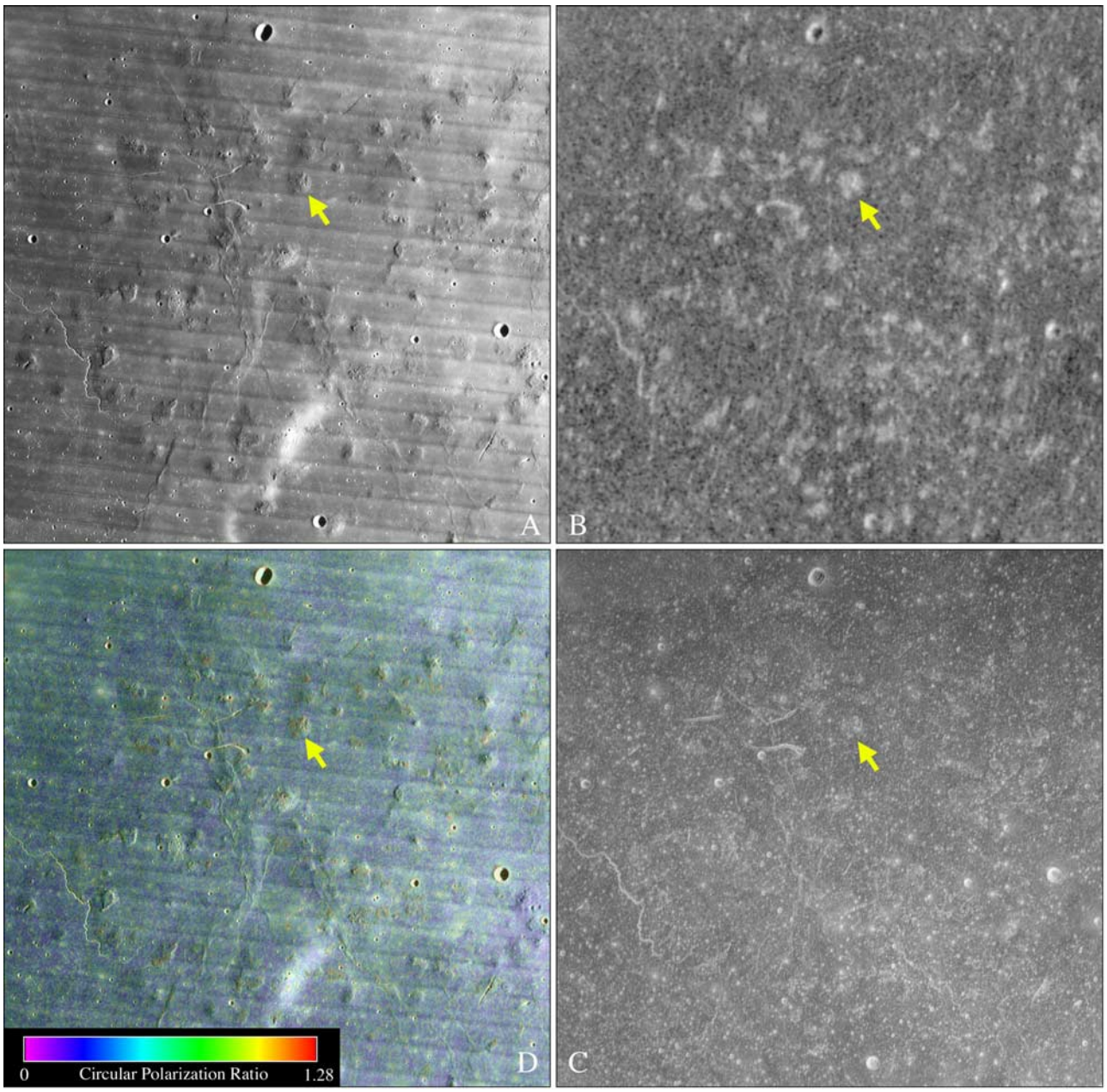

Figure 2. Photo and radar image data for the Marius Hills. (a) Lunar Orbiter IV photo, showing a portion of the high-albedo Reiner Gamma Formation at lower center; (b) 70-cm same-sense circular polarization backscatter image; (c) 12.6-cm same-sense circular polarization backscatter image; (d) 12.6-cm circular polarization ratio values as color overlay on Lunar Orbiter IV-157/H2 image. Yellow arrows denote location of dome shown in Figure 3.

data to a final maximum uncertainty of 3 dB among images collected on different days [*Campbell et al.*, 2007]. Across any single imaged area, the relative values of the 70-cm backscatter strength are very well calibrated (<1 dB). We have not yet calibrated the 12.6-cm data to σ^0 values, so we limit discussions here to relative differences among nearby geologic features.

[9] Comparisons to terrestrial features are enabled by data from the NASA/JPL AIRSAR system, which collected multipolarization backscatter measurements for many volcanic surfaces at 5.7-cm, 24-cm, and 68-cm wavelengths [e.g., *Campbell et al.*, 1993; *Campbell and Shepard*, 1996; *Plaut et al.*, 2004]. The relative calibration of σ^0 values among various terrestrial sites, across the AIRSAR wavelengths, and within the lunar 70-cm data set, again all have an uncertainty of perhaps 2–3 dB, so we rely primarily on the well-calibrated CPR values [e.g., *Freeman et al.*, 1992] as a comparative parameter.

3. Marius Hills

[10] We examine a portion of the Marius Hills dome complex north of Reiner crater (Figure 2a). Domes in this region include both the "low" (50–100 m high) and

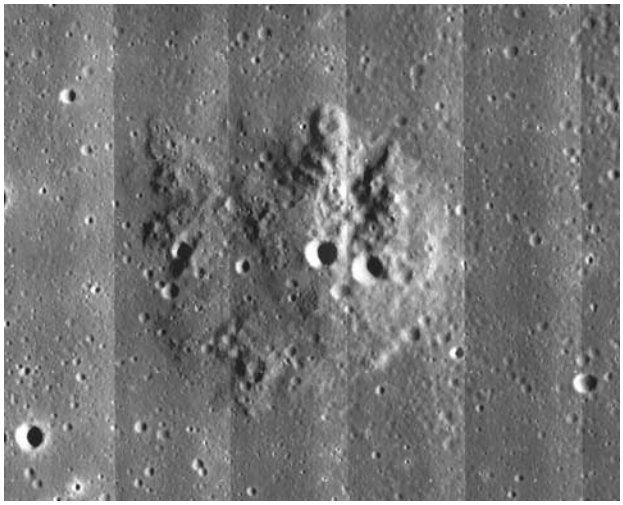

Figure 3. Lunar Orbiter photo (V-214) of a steep-sided dome in the Marius Hills ~8.5 km in diameter, shown by yellow arrows in Figure 2. Note the lobate structures to the north and northwest, suggesting emplacement as viscous lava flows.

"steep-sided" (up to 250 m high) types noted by *Guest* [1971]. Even at 500-m spatial resolution, it is clear that the domes are characterized by much higher (up to 10 dB, or a factor of 10 in power) 70-cm SC backscatter than the nearby mare plains (Figure 2b). At 12.6-cm wavelength, the domes have a much lower, but consistent, SC echo contrast with the mare background (Figure 2c). These properties are well illustrated by a steep-sided, 8.5-km diameter dome at 14°N, 55°W (Figure 3, and marked by yellow arrow on each plot of Figure 2).

[11] The 12.6-cm radar signals penetrate up to a meter or two in typical mare regolith, with shallower probing for more ilmenite-rich source material, and are sensitive to surface and suspended rocks about 2 cm and larger in diameter. The 70-cm data reach about a factor of five times greater depth for any given ilmenite content, and are sensitive to rocks of diameter about 10 cm and larger. The SC echo contrast with the nearby maria suggests a greatly increased abundance of scattering elements (rocks or rugged terrain) on the surface or within the probing range of the 70-cm signals (5–10 m). The smaller radar enhancement at 12.6 cm implies that such rocks or rough terrain are below the surface, mantled by a meter or so of regolith that preferentially attenuates the shorter radar wavelength.

[12] A more quantitative sense of the near-surface roughness and/or rock abundance on the domes may be gained from a comparison of their CPR values with other lunar and terrestrial geologic features. At 12.6-cm wavelength (Figure 2d), the domes have local μ_c values that reach 1.2 or slightly higher (where the SC and OC power values have been spatially averaged over 192 total "looks" to reduce speckle-induced uncertainty to about 7%). Such values do not appear to be solely linked with postemplacement impact craters or steep dome margins, but are a characteristic of parts of the upper dome surfaces. The nearby maria have area-averaged values of 0.2–0.4, but similarly high (>1) values are noted for the near-rim ejecta of many apparently young impact craters in the region. The 70-cm data have lower spatial resolution, so we averaged over boxes that encompassed large fractions of any given dome surface and kept the speckle-induced uncertainty in the CPR to <10%. The steep-sided dome in Figure 3 has an average 70-cm μ_c value of 0.84, and a survey of seven other domes large enough for valid CPR estimates yielded a range from 0.48 to 0.91 (again at worst ± 0.1).

[13] We first compare the 70-cm CPR values for the Marius domes with those of near-rim ejecta from 15 large, young impact craters across the nearside (Figure 4). Averages of SC and OC echo power over boxes 10 × 10 km and greater yield μ_c values of 0.57 to 1.34, and local values at the few kilometer scale can be even higher (Figure 5). Variations in CPR among these craters are due to a combination of differences in radar incidence angle (lower angles lead to smaller μ_c due to increased quasi-specular scatter in the OC channel), crater age (greater age enhances micrometeorite breakdown of surface blocks) [*Thompson et al.*, 1979, 1980], and target material (higher-ilmenite material allows less radar penetration and volume scattering).

[14] Similarly, high CPR values are also observed in rugged settings on the Earth. We use AIRSAR measurements to illustrate the range of polarization ratio behavior as a function of radar wavelength for three types of rough terrain: the December 1974 a′a lava flow on Kilauea Volcano, Hawaii [*Gaddis et al.*, 1990], the basaltic-andesite SP flow in northern Arizona [*Schaber et al.*, 1980], and the near-rim ejecta of Meteor Crater, Arizona (Figure 6). A smooth area of pahoehoe lava from the December 1974 eruption was included to illustrate the low end of the roughness range. In each case, we averaged the SC and OC echo power values over at least 300 "looks" in order to reduce the speckle uncertainty in μ_c to less than about 6%.

[15] The various rough surfaces have different CPR behaviors with illuminating wavelength (Figure 7), which we attribute to the degree and form of wavelength-scale structure. The December 1974 pahoehoe and a′a surfaces have gradually decreasing μ_c values with longer wavelength, consistent with the often observed decline in surface roughness at longer spatial scales [*Shepard et al.*, 2001]. The rugged a′a flow has an average CPR of about 0.4 at 68-cm wavelength, below the range of the Marius domes and young impact crater values (Figure 4). Polarization ratios are much higher (up to about unity) in the Meteor Crater near-rim ejecta and on the blocky SP lava flow, but the two sites have a different wavelength dependence in their CPR values. We speculate that this difference is due to the size-frequency distribution of blocks at the two sites. On SP flow, the maximum rock face size is about a meter, but in the part of the Meteor Crater deposits sampled here the blocks can be several meters in diameter. This may permit effective multiple-bounce scattering even at longer wavelengths, where at SP there are fewer smooth, facet-like reflectors on the scale of the 68-cm radar signal. In any case, it is clear from the AIRSAR data that circular polarization ratio values of unity or slightly higher can be generated by blocky, rugged terrain. The dry lunar regolith should permit greater radar penetration and volume scattering than the soil around Meteor Crater, enhancing the probability of subsurface multiple scattering events (Appendix) that further raise the CPR to the values noted

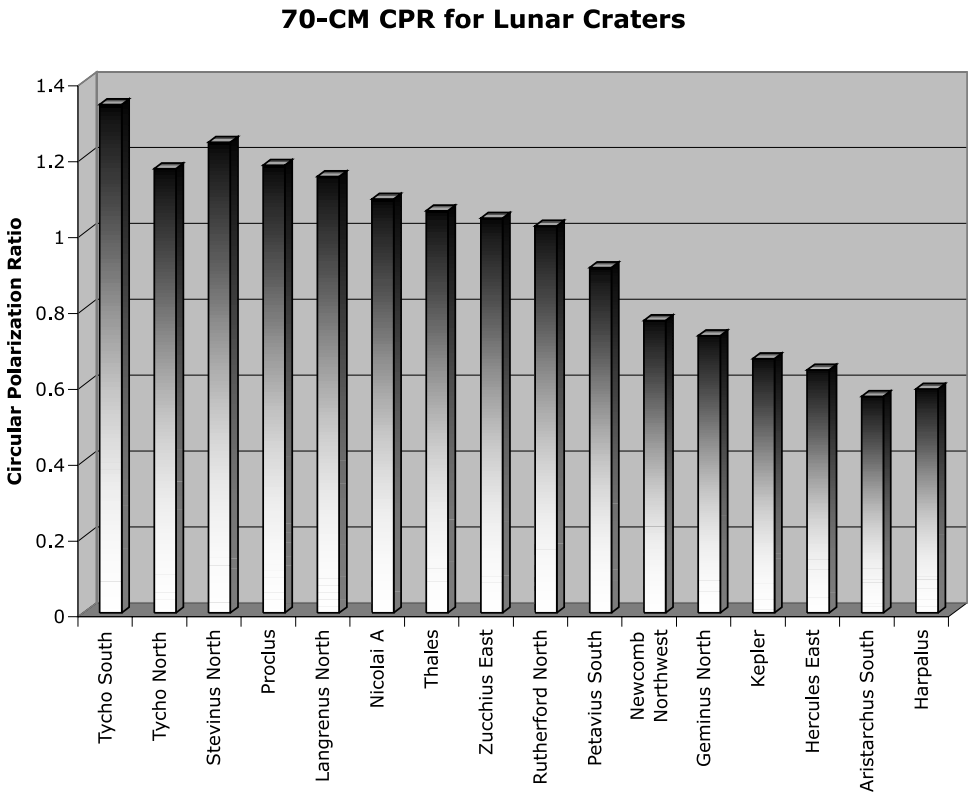

Figure 4. Circular polarization ratio (CPR) at 70-cm wavelength for near-rim ejecta of Eratosthenian- to Copernican-aged craters on the lunar nearside. Variations in CPR are attributed to a combination of radar incidence angle, crater age, and target materials.

for Tycho (Figure 5) and other young craters. The μ_c range observed for the Marius domes, 0.48 to 0.91, is consistent with values observed for young crater ejecta and the blocky SP flow deposit, supporting the premise that the domes are characterized by significantly greater near-surface rock abundance or more rugged terrain than typical mare lava flows.

4. Mons Rümker

[16] Mons Rümker is an 80-km diameter collection of coalesced domes and steep-margined flows that are embayed by later basalts of northern Oceanus Procellarum (Figure 8a). *Guest* [1971] divides the domes and flows into four groups based on their relative age, such that the steeper southern domes are the youngest, and the oldest unit defines much of the lateral extent of the complex where it overlies or embays the lineated northern terrain. The radar properties of Mons Rümker are considerably different from those of the Marius Hills, and have more in common with features seen on the Aristarchus Plateau [*Campbell et al.*, 2008]. SC polarization radar echoes (Figure 8c) and CPR values (Figure 8d) at 12.6-cm wavelength are generally lower than

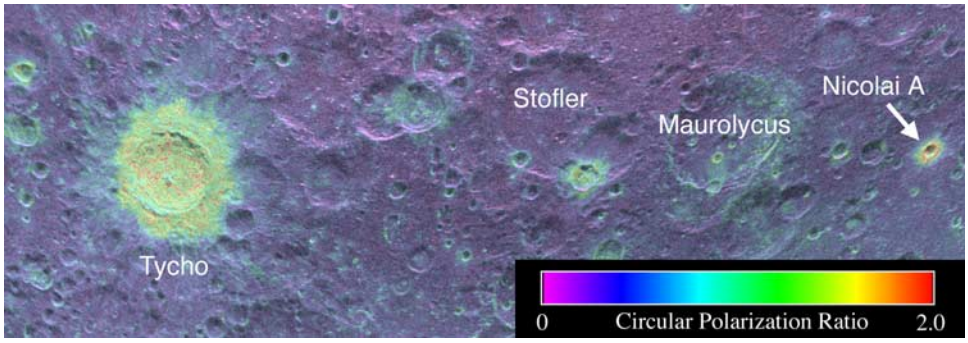

Figure 5. Color overlay of 70-cm circular polarization ratio for part of the southern lunar highlands on opposite-sense circular polarization radar image. Note the occurrence of CPR values consistently >1 in the Tycho crater (85 km diameter) ejecta and floor, with localized values of up to two. A total of 175 radar looks are averaged for each CPR value, so the speckle-related uncertainty is about 8%. The young crater Nicolai A (13 km diameter) also has very high CPR values in its near-rim ejecta.

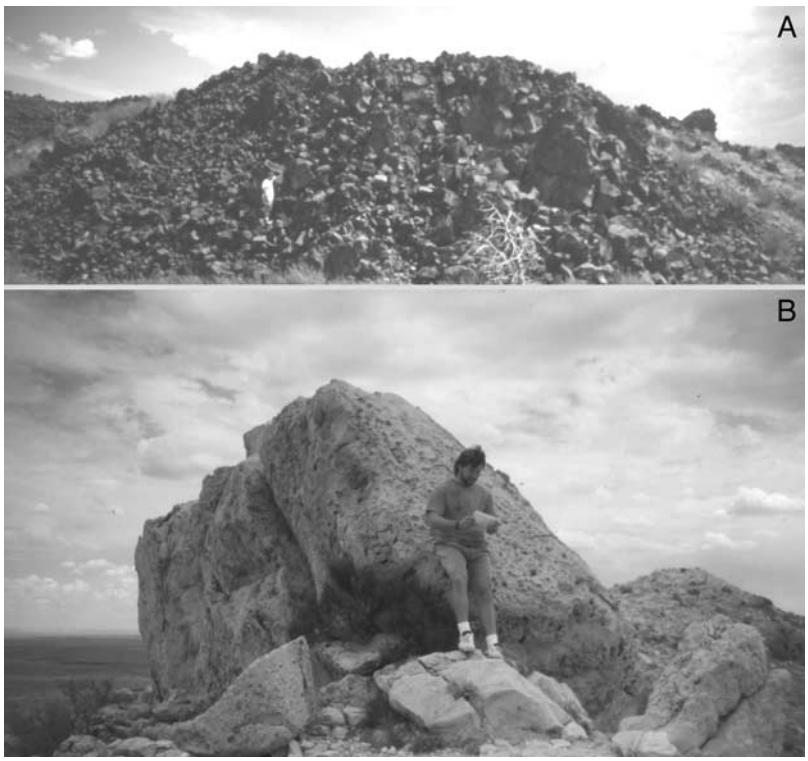

Figure 6. Photos of two field sites used as examples for AIRSAR data in Figure 8. (a) SP flow in northern Arizona, with person for scale at middle left. Typical blocks making up this flow are 50 cm and larger in scale. (b) Large ejecta blocks on the rim of Meteor Crater, Arizona.

the surrounding maria across the entire complex, with the exception of young, radar bright impact craters. The 70-cm SC echoes are very low in the northern area mapped as Fra Mauro material, and low to moderately low in the southern part of the dome complex (Figure 8b). A region of moderate to high radar brightness, however, extends from the north central part of Mons Rümker to the end of the northeastern "tongue," the largest Fra Mauro outlier mapped by *Guest* [1971] (Figure 9).

[17] Estimates of FeO and TiO_2 content from models that use Clementine multispectral data [*Lucey et al.*, 2000; *Gillis et al.*, 2003] show that Mons Rümker has a mare-like iron signature (Figure 10, middle), in contrast to the highlands dominated, low-FeO terrain surrounding Sinus Iridum [see also *Weitz and Head*, 1999]. The relatively high FeO signature (~15%) of Mons Rümker suggests that the lineated terrain mapped as Fra Mauro Formation cannot expose significant highlands material at the surface. TiO_2 abundances are low across the dome complex, with the lowest values generally occurring in the east-west trending central region of higher 70-cm backscatter. The surrounding mare lava flows vary widely in their TiO_2 abundance (Figure 10, bottom), and in general the 70-cm radar echoes (Figure 10, top) are inversely correlated with inferred greater ilmenite ($FeTiO_3$) content [cf. *Schaber et al.*, 1975; *Campbell et al.*, 1997]. The 70-cm echoes from northern and southern Mons Rümker, however, are lower than observed for much higher-titanium mare units just to the east. The TiO_2 retrieval algorithm is not well calibrated for potentially glass-rich deposits, but a range of 1–3 weight percent TiO_2 was also derived on the basis of neutron spectrometer data [*Elphic et al.*, 2002]. Assuming that the TiO_2 abundance, and thus the microwave loss tangent, is relatively low [*Campbell et al.*, 2008], the low 12.6-cm radar echoes imply a very small population of surface and suspended rocks larger than about 2 cm in diameter within the upper meter or two, and the very low

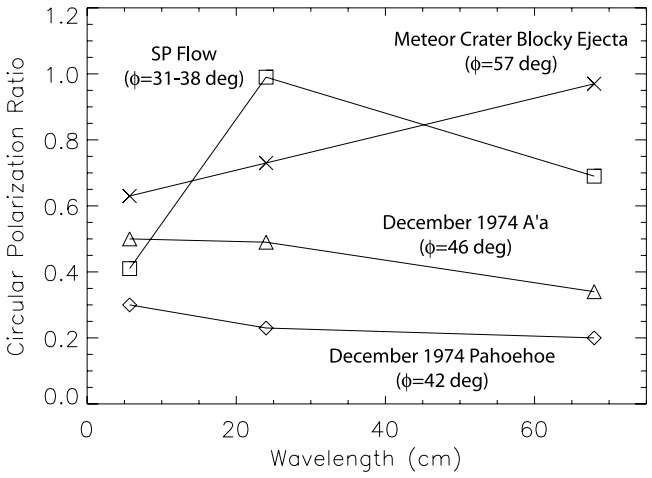

Figure 7. Circular polarization ratio versus radar wavelength for four terrestrial sites that exhibit a wide range of surface roughness properties. Radar incidence angle, φ, for each site is noted.

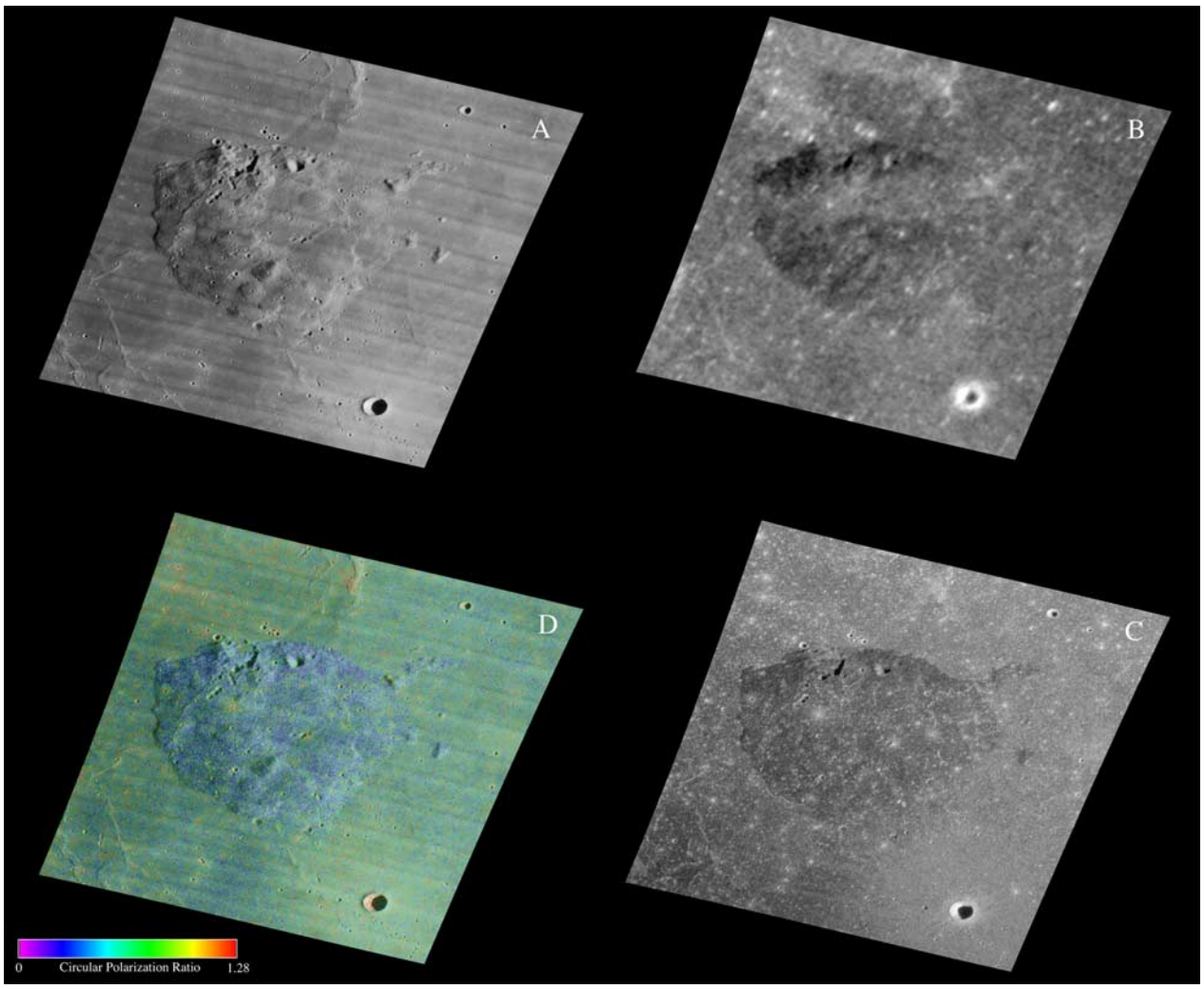

Figure 8. Mosaic of photo and radar image data for Mons Rümker (~80 km diameter). (a) Lunar Orbiter photo IV-163/H2; (b) 70-cm same-sense circular polarization backscatter image; (c) 12.6-cm same-sense circular polarization backscatter image; (d) 12.6-cm circular polarization ratio values as color overlay on Lunar Orbiter image.

70-cm returns in the northern and southern areas suggest minimal decimeter-scale and larger rocks within the upper 5–10 m.

[18] We propose that the lineated terrain in the north, and probably the entire dome complex, is mantled by several meters of fine-grained, rock-poor material of basaltic composition, consistent with the observation of subdued relief by *Smith* [1974]. A pyroclastic origin, similar to that of thick mantling units on the Aristarchus Plateau, seems most likely. Support for this interpretation is provided by multispectral studies, which show that several small craters in the lineated terrain expose highlands material from beneath a low-albedo surface [*Weitz and Head*, 1999]. The central area of higher 70-cm radar return has low 12.6-cm echoes, so we suggest that this area has a thinner mantle, and likely a more rugged substrate. A rough basal interface due to blocky morphology is reasonable on the basis of the properties of the Marius Hills, and the high radar echoes could indicate a

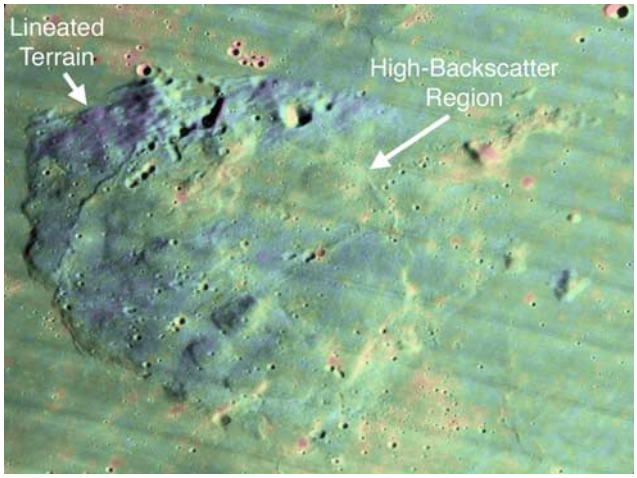

Figure 9. 70-cm same-sense circular polarization radar echoes shown as color overlay on Lunar Orbiter photo of Mons Rümker (about 80 km diameter). Blue tones indicate very low returns, while progressively stronger echoes are noted by green, yellow, and red tones.

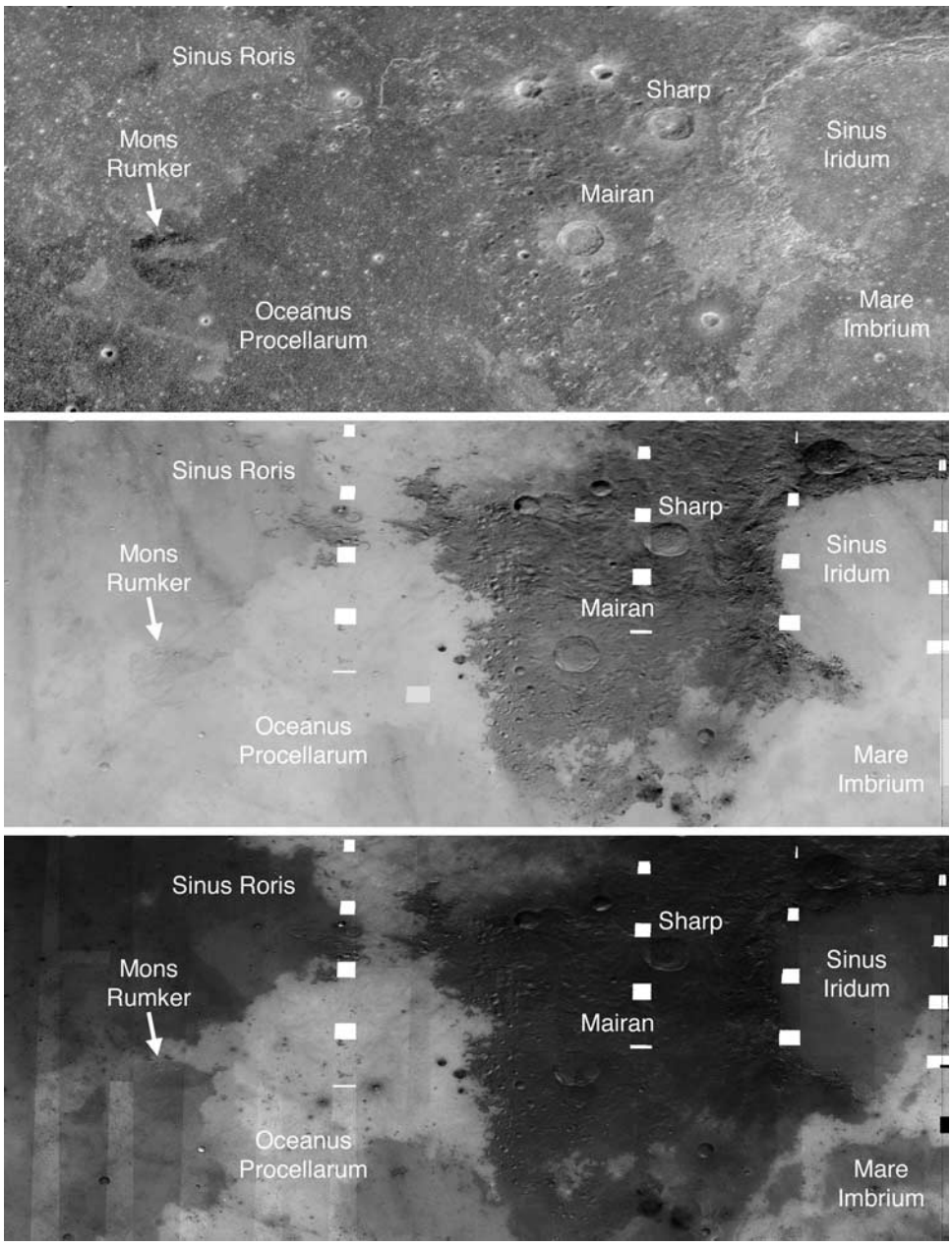

Figure 10. Regional views of northern Oceanus Procellarum and northwest Mare Imbrium: (top) 70-cm same-sense circular polarization radar image; (middle) FeO abundance (5–22% range from black to white) from model based on Clementine multispectral data [*Lucey et al.*, 2000]; (bottom) TiO_2 abundance (0–15% range from black to white) based on model of *Gillis et al.* [2003]. The 70-cm radar echoes from northern and southern Mons Rümker are much lower than those of mare basalt flows with similar estimated TiO_2 content.

rugged flow unit linked with the low-relief dome in the northeast quadrant of Mons Rümker (Figure 9).

5. Conclusions

[19] The Marius domes are characterized by high backscatter relative to the maria, especially at 70-cm wavelength, and by high CPR values at both 12.6-cm and 70-cm wavelengths. We use these high values and their consistency with the properties of near-rim, young crater ejecta, to infer rugged flow morphology beneath a meter or two of mantling regolith. The mare regolith is produced by impact fragmentation of an originally competent basalt layer to produce a mixture of rocks of varying diameter in a fine-grained matrix. Younger mare units have a thinner, more rocky regolith, and thus a higher σ^0_{SC} and CPR for any given microwave loss characteristics [*Campbell et al.*, 1997]. This process yields maximum 70-cm μ_c values for the maria of $\sim$0.4, below the range observed for the Marius domes. It is thus unlikely that the radar scattering properties of the

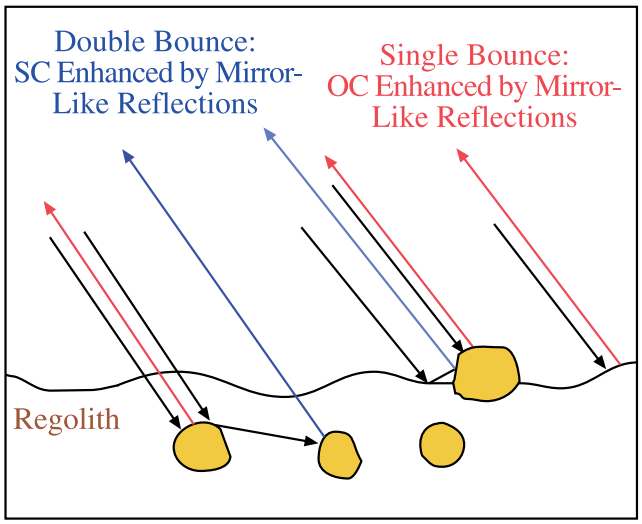

Figure A1. Cartoon of radar scattering from regolith with surface and suspended rocks. Incident radar signals represented by black arrows. Single-bounce backscatter (noted by red arrows) has an opposite-sense circular (OC) polarization mirror-like echo and roughly equal components of OC and same-sense (SC) returns related to scattering from wavelength-scale discontinuities like rock edges. Double-bounce backscattering (noted by blue arrows) has similar OC and SC returns due to wavelength-scale roughness, but any facet-like double reflections are strongly polarized in the SC sense that may increase the observed circular polarization ratio (SC/OC).

domes could arise by small impact reworking of a smooth lava flow surface.

[20] We conclude that the dome-forming flows had an initial morphology distinct from mare-forming units, and most likely similar to blocky terrestrial deposits like SP. The Marius domes are not similar to the steep-sided "pancake" domes on Venus, which have relatively smooth upper surfaces and are inferred to form by slow extrusion of basalt [*Stofan et al.*, 2000]. If magma compositions with enhanced silica content are implausible on the basis of lunar sample studies, then the blocky structure of the dome-forming lava must arise from some combination of compositional change, effusion rate, and/or cooling effects not typically observed in basaltic landforms on Earth. Similarly rugged lava flow morphology may characterize at least the east central portion of Mons Rümker, which appears to have had significant pyroclastic eruptions late in its geologic history.

Appendix A: Circular Polarization Ratio

[21] The circular polarization ratio, μ_c, is defined as the ratio of the backscattered power in the same-sense circular (SC) to the opposite-sense circular (OC) modes. In general, the OC echo is dominated at small incidence angles, φ, by strong, mirror-like (quasi-specular) reflections from gently tilted areas of the surface that are many times the illuminating wavelength, λ, in extent. As φ increases, there are fewer such large-scale facets, but there remains a lower OC echo component arising from rock faces and other features that are locally smooth on length scales comparable to λ. At the same time, reflections from rock edges and other sharp terrain features create "diffuse" echoes that are split about evenly between the SC and OC channels. Since the OC reflection also contains the facet-like component, any combination of single-scattering events (noted by the red ray-paths in Figure A1) from the surface or from objects suspended within the probing range of the radar signal leads to $\mu_c < 1$, with diminishing CPR for lower φ.

[22] The CPR may increase owing to double-bounce scattering between the surface and rock faces, or between rocks suspended within a regolith (the blue paths in Figure A1). The sense of circular polarization is reversed upon each mirror-like reflection, so a signal scattered back to the observer after two such events will have a strong SC component. There will also be an increase in the diffuse echo component (SC = OC) due to these interactions. How such a mechanism, however, can lead to $\mu_c > 1$ is uncertain. The backscattered power for a two-bounce geometry is proportional to ρ^2, where ρ is the effective reflection coefficient of the rocks in the relevant background medium (vacuum/air or regolith). Single-bounce echoes are proportional to ρ, so for a typical reflectivity of 0.1 the difference is a factor of 10 in power. High CPR values are observed to arise in radar backscattering from thick deposits of water ice with internal cracks or voids, attributed to a factor-of-two enhancement of backscattered SC signals by coherent superposition of rays that follow the same path through the medium in opposite directions [e.g., *Ostro et al.*, 1992; *Black et al.*, 2001]. Echoes generated by two or more bounces between relatively smooth rock faces would exhibit the same effect, at least partly offsetting the effect of diminished net reflectivity.

[23] Our study, and other recent work [*Campbell and Campbell*, 2006; *Campbell et al.*, 2006] shows that it is relatively common on the Earth and Moon, in geologic settings where rocks are closely spaced at the surface or comprise a dense population suspended within the probing range of the radar signal, to observe CPR values of unity or greater. In general, multiple-scattering interactions between irregular objects on the scale of the radar wavelength or larger are not well represented in current theoretical models. Further work is required to understand the possible mechanisms by which strong SC-polarized echoes arise in these environments.

[24] **Acknowledgments.** We thank two anonymous reviewers who provided helpful comments on the manuscript. This work was supported in part by a grant from NASA's Planetary Geology and Geophysics Program. The authors thank the staff at Arecibo Observatory and the Green Bank Telescope for invaluable assistance in collecting the lunar radar data. In particular, we thank F. Ghigo at the GBT and M. Nolan at Arecibo. J. Chandler of SAO provided ephemeris data for the observations. The Arecibo Observatory is part of the National Astronomy and Ionosphere Center, which is operated by Cornell University under a cooperative agreement with the National Science Foundation. The National Radio Astronomy Observatory is a facility of the National Science Foundation operated under cooperative agreement by Associated Universities, Inc.

References

Black, G. J., D. B. Campbell, and P. D. Nicholson (2001), Icy Galilean satellites: Modeling radar reflectivities as a coherent backscatter effect, *Icarus*, *151*, 167–180, doi:10.1006/icar.2001.6616.

Campbell, B. A., and D. B. Campbell (2006), Surface properties in the south polar region of the Moon from 70-cm radar polarimetry, *Icarus*, *180*, 1–7, doi:10.1016/j.icarus.2005.08.018.

Campbell, B. A., and B. R. Hawke (2005), Radar mapping of lunar cryptomaria east of Orientale basin, *J. Geophys. Res.*, *110*, E09002, doi:10.1029/2005JE002425.

Campbell, B. A., and M. K. Shepard (1996), Lava flow surface roughness and depolarized radar scattering, *J. Geophys. Res.*, *101*, 18,941–18,952, doi:10.1029/95JE01804.

Campbell, B. A., R. E. Arvidson, and M. K. Shepard (1993), Radar polarization properties of volcanic and playa surfaces: Applications to terrestrial remote sensing and Magellan data interpretation, *J. Geophys. Res.*, *98*, 17,099–17,114, doi:10.1029/93JE01541.

Campbell, B. A., B. R. Hawke, and T. W. Thompson (1997), Long-wavelength radar studies of the lunar maria, *J. Geophys. Res.*, *102*, 19,307–19,320, doi:10.1029/97JE00858.

Campbell, B. A., D. B. Campbell, J. L. Margot, R. R. Ghent, M. Nolan, J. Chandler, L. M. Carter, and N. J. S. Stacy (2007), Focused 70-cm radar mapping of the Moon, *IEEE Trans. Geosci. Remote Sens.*, *45*(12), 4032–4042, doi:10.1109/TGRS.2007.906582.

Campbell, B. A., L. M. Carter, B. R. Hawke, D. B. Campbell, and R. R. Ghent (2008), Volcanic and impact deposits of the Moons Aristarchus Plateau: A new view from Earth-based radar images, *Geology*, *36*, 135–138, doi:10.1130/G24310A.1.

Campbell, D. B., B. A. Campbell, L. M. Carter, J. L. Margot, and N. J. S. Stacy (2006), Lunar polar ice: No evidence for thick deposits at the south pole, *Nature*, *443*, 835–837, doi:10.1038/nature05167.

Carrier, W. D., G. R. Olhoeft, and W. Mendell (1991), Physical properties of the lunar surface, in Lunar Sourcebook, edited by A. V. Markov, pp. 156–175, Cambridge Univ. Press, New York.

Elphic, R. C., D. J. Lawrence, W. C. Feldman, B. L. Baraclough, S. Maurice, P. G. Lucey, D. T. Blewett, and A. B. Binder (2002), The Lunar Prospector neutron spectrometer constraints on TiO_2, *J. Geophys. Res.*, *107*(E4), 5024, doi:10.1029/2000JE001460.

Freeman, A., J. J. van Zyl, J. D. Klein, H. A. Zebker, and Y. Shen (1992), Calibration of Stokes and scattering matrix format polarimetric SAR data, *IEEE Trans. Geosci. Remote Sens.*, *30*, 531–539, doi:10.1109/36.142931.

Gaddis, L. R., P. J. Mouginis-Mark, and J. N. Hayashi (1990), Lava flow surface textures: SIR-B radar image texture, field observations, and terrain measurements, *Photogramm. Eng. Remote Sens.*, *56*, 211–224.

Gillis, J. J., B. L. Joliff, and R. C. Elphic (2003), A revised algorithm for calculating TiO_2 from Clementine UVVIS data: A synthesis of rock, soil, and remotely sensed TiO_2 concentrations, *J. Geophys. Res.*, *108*(E2), 5009, doi:10.1029/2001JE001515.

Greeley, R. (1971), Lava tubes and channels in the lunar Marius Hills, *Moon*, *3*, 289–314, doi:10.1007/BF00561842.

Guest, J. E. (1971), Centres of igneous activity in the maria, in *Geology and Physics of the Moon*, edited by G. Fielder, pp. 41–53, Elsevier, New York.

Hagfors, T. (1967), A study of the depolarization of lunar radar echoes, *Radio Sci.*, *2*, 445–465.

Heather, D. J., S. K. Dunkin, and L. Wilson (2003), Volcanism on the Marius Hills plateau: Observational analyses using Clementine multispectral data, *J. Geophys. Res.*, *108*(E3), 5017, doi:10.1029/2002JE001938.

Lucey, P. G., D. T. Blewett, and B. D. Joliff (2000), Lunar iron and titanium abundance algorithms based on final processing of Clementine UV-visible images, *J. Geophys. Res.*, *105*, 20,297–20,306, doi:10.1029/1999JE001117.

McCauley, J. F. (1967), Geology of the Moon, Hevelius region, in *USGS Geologic Atlas of the Moon*, sheet I-491 (LAC-56), U.S. Geol. Surv., Reston, Va.

Ostro, S. J., et al. (1992), Europa, Ganymede, and Callisto: New radar results from Arecibo and Goldstone, *J. Geophys. Res.*, *97*, 13,091–13,102.

Plaut, J. J., S. W. Anderson, D. A. Crown, E. R. Stofan, and J. van Zyl (2004), The unique radar properties of silicic lava domes, *J. Geophys. Res.*, *109*, E03001, doi:10.1029/2002JE002017.

Rutherford, M. J., P. C. Hess, and G. H. Daniel (1974), Experimental liquid line of descent and liquid immiscibility for basalt 70017, *Proc. Lunar Sci. Conf.*, *5th*, 569–583.

Schaber, G. G., T. W. Thompson, and S. H. Zisk (1975), Lava flows in Mare Imbrium: An evaluation of anomalously low Earth-based radar reflectivity, *Moon*, *13*, 395–423, doi:10.1007/BF02626384.

Schaber, G. G., C. Elachi, and T. G. Farr (1980), Remote sensing of SP mountain and SP lava flow in North-central Arizona, *Remote Sens. Environ.*, *9*, 149–170, doi:10.1016/0034-4257(80)90005-X.

Scott, D. H., and R. E. Eggleton (1973), Geologic map of the Rumker quadrangle of the Moon, in *USGS Geologic Atlas of the Moon*, sheet I-805 (LAC 23), U.S. Geol. Surv., Reston, Va.

Shepard, M. K., B. A. Campbell, M. Bulmer, T. Farr, L. R. Gaddis, and J. Plaut (2001), The roughness of natural terrain: A planetary and remote sensing perspective, *J. Geophys. Res.*, *106*, 32,777–32,795.

Smith, E. I. (1974), Rumker Hills: A lunar volcanic done complex, *Moon*, *10*, 175–181, doi:10.1007/BF00655718.

Stofan, E. R., S. W. Anderson, D. A. Crown, and J. J. Plaut (2000), Emplacement and composition of steep-sided domes on Venus, *J. Geophys. Res.*, *105*, 26,757–26,772, doi:10.1029/1999JE001206.

Thompson, T. W., W. J. Roberts, W. K. Hartmann, R. W. Shorthill, and S. H. Zisk (1979), Blocky craters: Implications about the lunar megaregolith, *Moon Planets*, *21*, 319–342, doi:10.1007/BF00897360.

Thompson, T. W., J. A. Cutts, R. W. Shorthill, and S. H. Zisk (1980), Infrared and radar signatures of lunar craters: Implications about crater evolution, *Geochim. Cosmochim. Acta*, *S12*, 483–499.

Weitz, C. M., and J. W. Head (1999), Spectral properties of the Marius Hills volcanic complex and implications for the formation of lunar domes and cones, *J. Geophys. Res.*, *104*, 18,933–18,956, doi:10.1029/1998JE000630.

Whitford-Stark, J. L., and J. W. Head (1977), The Procellarum volcanic complexes: Contrasting styles of volcanism, *Proc. Lunar Planet. Sci. Conf., 8th*, *2*, 705–2724.

B. A. Campbell, Center for Earth and Planetary Studies, Smithsonian Institution, MRC 315, P.O. Box 37012, Washington, DC 20013-7012, USA. (campbellb@si.edu)

D. B. Campbell, Department of Astronomy, 610 Space Sciences Building, Cornell University, Ithaca, NY 14853, USA.

B. R. Hawke, Hawai'i Institute of Geophysics and Planetology, 1680 East-West Road, School of Ocean and Earth Science and Technology, University of Hawai'i, Honolulu, HI 96822, USA.